

to the optic disc (fig. 3a). The arm-to-retina time of the fluorescein angiography (fig. 3b) was delayed, and an island-like hypofluorescence surrounded by a hyperfluorescent region was present inferior to the optic disc.

Multifocal ERGs (mfERGs) and multifocal VEPs (mfVEPs) were recorded approximately two weeks after the surgery according to the ISCEV standard [14, 15]. The amplitudes of the mfERGs (fig. 4a) were within the normal range over the central retinal area, while the amplitudes of the mfVEPs (fig. 4b) were reduced and the implicit times prolonged especially those elicited by stimulating the superior hemifield of the right eye. These findings suggested that the VFD did not originate in the retinal inner and middle layer but was of ganglion cell origin.

The visual acuity improved to 1.2 in one month and has been stable for 12 years in the right eye, but the optic disc gradually became paler especially in the inferior region (fig. 3c). Fluorescein angiography (fig. 3d) showed a delayed arm-to-retina time and a semicircular hypofluorescent region inferior to the optic disc. The VFD remained unchanged for more than 12 years after the surgery (fig. 1b). Optical coherence tomography (Spectralis OCT, Heidelberg Engineering, Germany) performed 12 years after the vitrectomy demonstrated a selective atrophy of the nerve fiber layer inferior to the optic disc in the right eye (fig. 3e).

A re-examination of the PhNR of the photopic ERGs recorded at the initial examination showed that it was selectively reduced in the right eye (table 1 and table 2). These findings strongly supported our initial diagnosis of ION.

## Discussion

Several mechanisms have been reported to explain the VFDs after vitreous surgery: phototoxicity due to the bright light from the operating microscope or endoillumination [16, 17], intra- or postoperative fluctuations of the intraocular pressure and/or systemic blood pressure [18–20], mechanical stress on the optic nerve during the creation of a posterior vitreous detachment [21], chemico-physical stress on the retina by dry air during fluid-air exchange [3], retinal damage due to panretinal photocoagulation [22], optic nerve damage due to retrobulbar anesthesia [6–9], and damage to the optic nerve because of the compromised circulation associated with diabetes mellitus [23–25].

Our case was initially diagnosed with ION because of the acute superior horizontal VFD. The attenuated mfVEPs corresponding to the VFD and normal mfERGs suggested that the pathological site was not in the outer and middle layers of the retina but the ganglion cells and/or optic nerve. This supported our initial diagnosis.

Little information is available of cases that developed ION after vitrectomy [18, 26]. Pendergast et al. [18] reported on a 73-year-old woman with coronary artery disease who developed ION 4 months after vitrectomy. Taban et al. [26] reported on two cases, a 65-year-old woman with hypertension and diabetes mellitus who developed ION at 3.5 weeks after vitrectomy, and a 94-year-old man with hypertension whose visual acuity was found to be reduced on postoperative day 34. Both were diagnosed with ION but the etiology of the ION was not determined. Taban et al. [26] also found 190 cases that developed a VFD after vitrectomy, and approximately 20% of these had evidence of optic nerve damage, relative afferent pupillary defect, or optic nerve pallor. They stated that in spite of the fact that the etiology of the VFD remains undetermined, VFD as a complication of vitreous surgery is relatively common. We suggest that circulatory disturbances associated with diabetes mellitus might have played some part in our case.

No obvious difference was found between the mfERGs from the superior and inferior retina which also supports our suggestion that the VFD did not originate in the inner and middle retinal layer but was of ganglion cell and/or optic nerve origin. Furthermore, the selectively reduced PhNR in the right eye strongly supported this idea, although we did not use this test in 1998. The PhNR has been reported to be a sensitive test to determine functional alterations of ganglion cells, and its clinical application has been extended [27–29]. Our case highlights the importance of the PhNR in differentiating ganglion cell damage in patients with VFD after surgery. It is, however, difficult to determine whether the ganglion cells or optic nerve was the exact origin in the present case. We believe that it is more likely that the ganglion cell damage was related to ION.

In summary, electrophysiological evaluations were helpful in making a diagnosis in our case. The mfERGs, mfVEPs, and PhNR were useful in determining the pathological site of the VFD that occurred after vitrectomy.

### Acknowledgements

Support of this study was provided by Research Grants on Sensory and Communicative Disorders from the Ministry of Health, Labor, and Welfare, Japan.

### Disclosure Statement

No author has a financial or proprietary interest in any material or method mentioned.

**Table 1.** Amplitude and implicit time of the P-100 in flash VEPs

Stimulus intensity	Right		Left		R-L	
	Amp., $\mu$ V	Imp.T., ms	Amp., $\mu$ V	Imp.T., ms	Amp., $\mu$ V	Imp.T., ms
0.3 J						
ND-3	3.4	130	2.4	138	1.00	-8.00
ND-2	5.4	117.5	5	130	0.40	-12.50
ND-1	6.3	127.5	11.6	130	-5.30	-2.50
ND-0	9.9	126.3	8.9	125	1.00	1.30
2.0 J	4.9	105	5.6	105	-0.70	0.00

Amp. = Amplitude; Imp.T. = implicit time.

**Table 2.** Amplitude and implicit time of the a- and b-waves and PhNR in each eye

Stimulus intensity	Right			Left			R-L										
	Amp., $\mu$ V			Imp.T., ms			Amp., $\mu$ V			Imp.T., ms							
	a-wave	b-wave	PhNR	a-wave	b-wave	PhNR	a-wave	b-wave	PhNR	a-wave	b-wave	PhNR	a-wave	b-wave			
0.3 J																	
ND-3	0	2.24	2.24	45	82.5		0.56	2.24	1.4	60	80		-0.56	0.00	0.84	-15.00	2.50
ND-2	0.56	0.84	2.8	80	90		1.68	3.36	1.96	47.5	90		-1.12	-2.52	0.84	32.50	0.00
ND-1	0	5.32	7.84	40	65		0.84	5.32	10.08	42.5	65		-0.84	0.00	-2.24	-2.50	0.00
ND-0	1	8.4	8.4	42.5	70		6.16	17.08	13.16	45	70		-5.16	-8.68	-4.76	-2.50	0.00
2.0 J																	
	6.16	14.56	12.04	37.5	60		7.28	17.08	23.8	45	67.5		-1.12	-2.52	-11.76	-7.50	-7.50

Amp. = Amplitude; Imp.T. = implicit time.

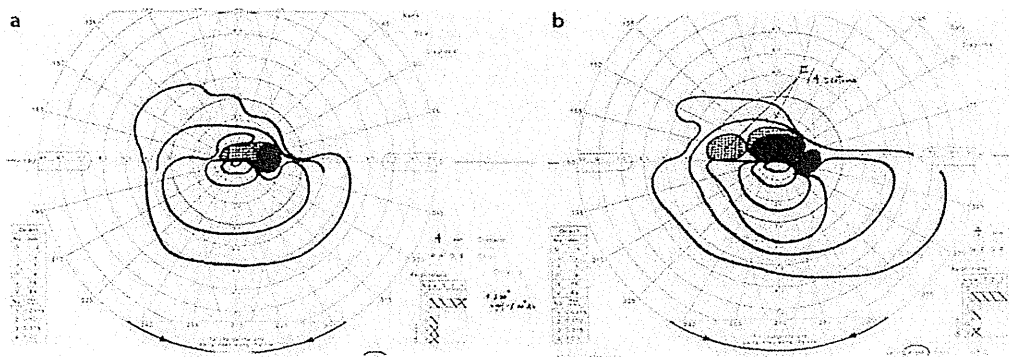


**Fig. 1.** Goldmann perimetry performed on the day after vitrectomy and again more than one year after surgery. The V-4 isopter is constricted in the superior and temporal-superior visual field, and the internal isopter shows a superior hemianopsia on the following day (a). The superior hemianopsia remained unchanged (b).

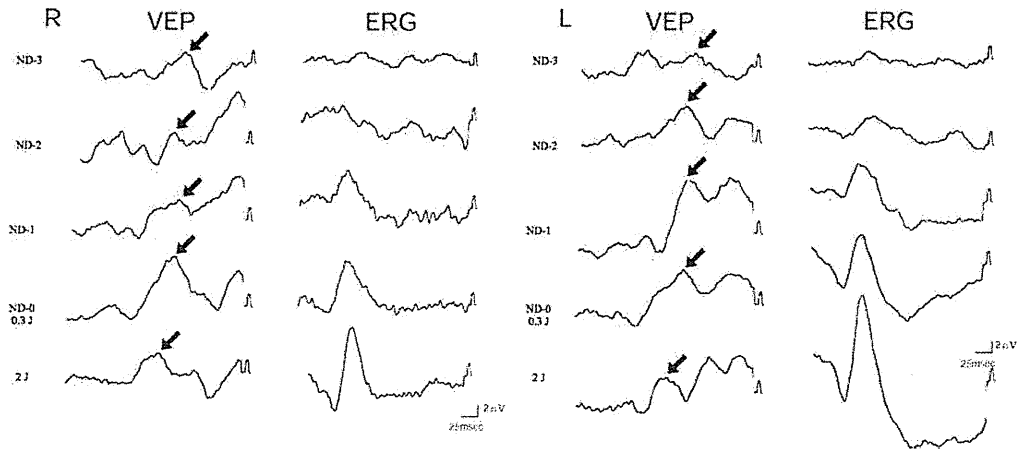


**Fig. 2.** Simultaneously recorded flash VEPs and full-field single-flash ERGs. No significant differences were found between the two eyes in the amplitude and implicit times of N-70 and P-100 in the flash VEPs. The photopic ERGs recorded with skin electrodes showed no obvious differences between the eyes in the amplitude and implicit times of the a- and b-waves, but the amplitudes of the PhNR were reduced in the right eye. The arrow points to P-100. The values of the amplitudes and implicit times are shown in table 1 and 2.

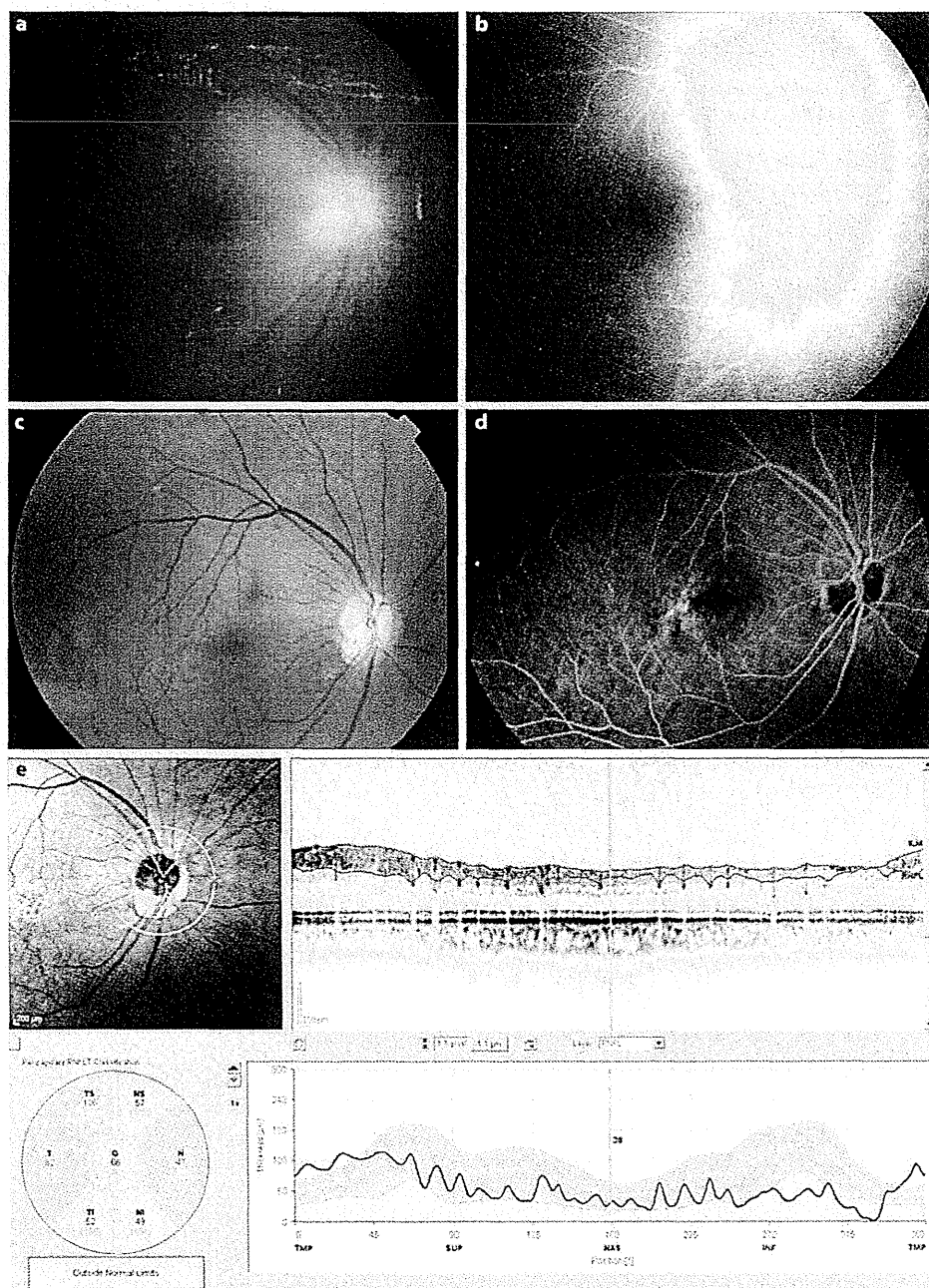


**Fig. 3.** Fundus photograph, fluorescein angiogram, and optical coherence tomographic images. **a** Fundus photograph taken one week after surgery showed localized edema adjacent to the optic disc. **b** Fluorescein angiogram obtained on the same day as that in **a** shows a delayed arm-to-retina time and island-like hypofluorescence surrounded by a hyperfluorescent region inferior to the optic disc. **c** Fundus photograph taken 10 years after surgery shows a pale optic disc especially in the inferior region. Visual acuity was 1.2. **d** Fluorescein angiogram obtained on the same day as **c** shows a delay in the arm-to-retina time and semicircular hypofluorescent region inferior to the optic disc. **e** The optic nerve fiber layer thickness analysis using optical coherence tomography (Spectralis OCT, Heidelberg Engineering, Germany) performed 12 years after vitrectomy showing selective atrophy of inferior nerve fiber layer around optic disc in the right eye.

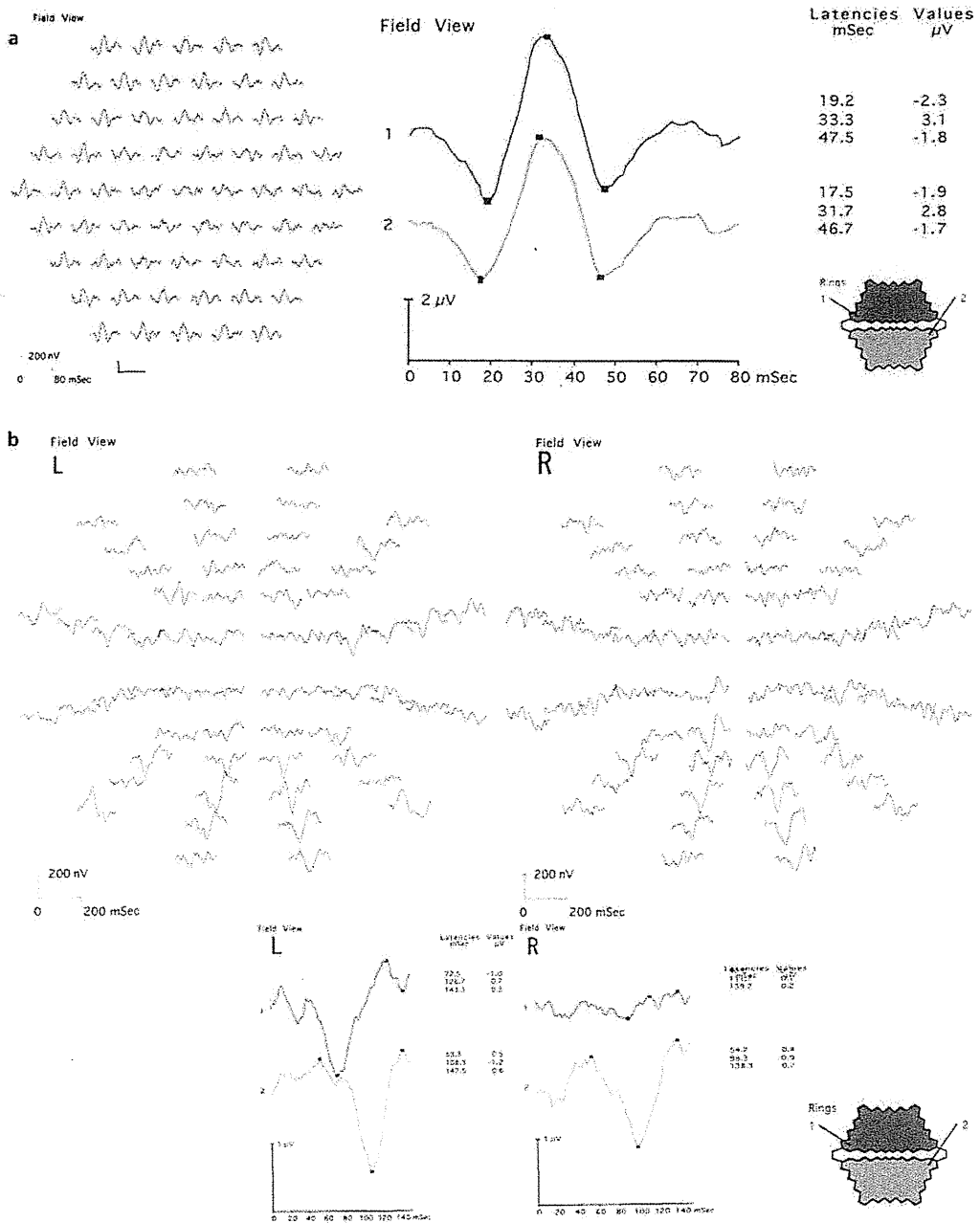


**Fig. 4.** Multifocal ERGs and VEPs recorded one week after the vitreous surgery. **a** The amplitudes and the implicit times of the mfERGs from the right eye are within the normal range. **b** The mfVEP showed amplitude reduction and delayed implicit time especially from superior hemifield in the right eye.

## References

- 1 Malinowski SM, Pesin SR: Visual field loss caused by retinal vascular occlusion after vitrectomy surgery. *Am J Ophthalmol* 1997;123:707–708.
- 2 Verma L, Venkatesh P, Tewari HK: Combined central retinal artery and central retinal vein occlusion following pars plana vitrectomy. *Ophthalmic Surg Lasers* 1999;30:317–319.
- 3 Melberg NS, Thomas MA: Visual field loss after pars plana vitrectomy with air/fluid exchange. *Am J Ophthalmol* 1995;120:386–388.
- 4 Yan H, Dhurjon L, Chow DR, Williams D, Chen JC: Visual field defect after pars plana vitrectomy. *Ophthalmology* 1998;105:1612–1616.
- 5 Welch JC: Dehydration injury as a possible cause of visual field defect after pars plana vitrectomy for macular hole. *Am J Ophthalmol* 1997;124:698–699.
- 6 Sullivan KL, Brown GC, Forman AR, Sergott RC, Flanagan JC: Retrobulbar anesthesia and retinal vascular obstruction. *Ophthalmology* 1983;90:373–377.
- 7 Cowley M, Campochiaro PA, Newman SA, Fogle JA: Retinal vascular occlusion without retrobulbar or optic nerve sheath hemorrhage after retrobulbar injection of lidocaine. *Ophthalmic Surg* 1988;19:859–861.
- 8 Devoto MH, Kersten RC, Zalta AH, Kulwin DR: Optic nerve injury after retrobulbar anesthesia. *Arch Ophthalmol* 1997;115:687–688.
- 9 Hamilton RC: A discourse on the complications of retrobulbar and peribulbar blockade. *Can J Ophthalmol* 2000;35:363–372.
- 10 Uemura A, Kanda S, Sakamoto Y, Kita H: Visual field defects after uneventful vitrectomy for epiretinal membrane with indocyanine green-assisted internal limiting membrane peeling. *Am J Ophthalmol* 2003;136:252–257.
- 11 Adachi M, Takahashi K, Nishikawa M, Miki H, Uyama M: High intraocular pressure-induced ischemia and reperfusion injury in the optic nerve and retina in rats. *Graefes Arch Clin Exp Ophthalmol* 1996;234:445–451.
- 12 Shinoda K, Ohde H, Ishida S, Kawashima S, Kitamura S, Mita S, Inoue M, Katsura H: A case of proliferative diabetic retinopathy with development of ischemic optic neuropathy after pars plana vitrectomy [in Japanese]. *Folia Ophthalmol Jpn* 2000;51:925–929.
- 13 Miyake Y, Hirose T, Hara A: Electrophysiologic testing of visual functions for vitrectomy candidates. I. Results in eyes with known fundus diseases. *Retina* 1983;3:86–94.
- 14 Hood DC, Bach M, Brigell M, Keating D, Kondo M, Lyons JS, Palmowski-Wolfe AM: ISCEV guidelines for clinical multifocal electroretinography (2007 edition). *Doc Ophthalmol* 2008;116:1–11.
- 15 Betsuin Y, Mashima Y, Ohde H, Inoue R, Oguchi Y: Clinical application of the multifocal VEPs. *Curr Eye Res* 2001;22:54–63.
- 16 Khwarg SG, Linstone FA, Daniels SA, Isenberg SJ, Hanscom TA, Geoghegan M, Straatsma BR: Incidence, risk factors, and morphology in operating microscope light retinopathy. *Am J Ophthalmol* 1987;103:255–263.
- 17 McDonald HR, Harris MJ: Operating microscope-induced retinal phototoxicity during pars plana vitrectomy. *Arch Ophthalmol* 1988;106:521–523.
- 18 Pendergast SD, McCuen BW 2nd: Visual field loss after macular hole surgery. *Ophthalmology* 1996;103:1069–1077.
- 19 Hayreh SS: Anterior ischemic optic neuropathy. IV. Occurrence after cataract extraction. *Arch Ophthalmol* 1980;98:1410–1416.
- 20 Jayam AV, Hass WK, Carr RE, Kumar AJ: Saturday night retinopathy. *J Neurol Sci* 1974;22:413–418.
- 21 Boldt HC, Munden PM, Folk JC, Mehaffey MG: Visual field defects after macular hole surgery. *Am J Ophthalmol* 1996;122:371–381.
- 22 Becker H, Schmitz J: Computer-assisted quantitative-static perimetry following panretinal argon laser coagulation in diabetic retinopathy [in German]. *Klin Monb] Augenheilkd* 1998;192:204–207.
- 23 Hidayat AA, Fine BS: Diabetic choroidopathy. Light and electron microscopic observations of seven cases. *Ophthalmology* 1985;92:512–522.
- 24 Kroll P, Wiegand W, Schmidt J: Vitreopapillary traction in proliferative diabetic vitreoretinopathy. *Br J Ophthalmol* 1909;83:261–264.
- 25 Langham ME, Grebe R, Hopkins S, Marcus S, Sebag M: Choroidal blood flow in diabetic retinopathy. *Exp Eye Res* 1991;52:167–173.

- 26 Taban M, Lewis H, Lee MS: Nonarteritic anterior ischemic optic neuropathy and 'visual field defects' following vitrectomy: could they be related? *Graefes Arch Clin Exp Ophthalmol* 2007;245:600–605.
- 27 Viswanathan S, Frishman LJ, Robson JG, Harwerth RS, Smith EL 3rd: The photopic negative response of the macaque electroretinogram: reduction by experimental glaucoma. *Invest Ophthalmol Vis Sci* 1999;40:1124–1136.
- 28 Gotoh Y, Machida S, Tazawa Y: Selective loss of the photopic negative response in patients with optic nerve atrophy. *Arch Ophthalmol* 2004;122:341–346.
- 29 Frishman LJ: Origins of the electroretinogram; in Heckenlively JR, Arden GB (eds): *Principle and Practice of Clinical Electrophysiology of Vision*, ed 2. Cambridge, Mass., The MIT Press, 2006, pp 139–183.



# Tropisms of AAV for Subretinal Delivery to the Neonatal Mouse Retina and Its Application for *In Vivo* Rescue of Developmental Photoreceptor Disorders

Satoshi Watanabe<sup>1,2,3,4</sup>, Rikako Sanuki<sup>1,2,3</sup>, Shinji Ueno<sup>5</sup>, Toshiyuki Koyasu<sup>5</sup>, Toshiaki Hasegawa<sup>6</sup>, Takahisa Furukawa<sup>1,2,3\*</sup>

**1** Laboratory for Molecular and Developmental Biology, Institute for Protein Research, Osaka University, Suita, Osaka, Japan, **2**JST, CREST, Suita, Osaka, Japan, **3** Department of Developmental Biology, Osaka Bioscience Institute, Suita, Osaka, Japan, **4** Kyoto University Graduate School of Medicine, Sakyo-ku, Kyoto, Kyoto, Japan, **5** Department of Ophthalmology, Nagoya University Graduate School of Medicine, Showa-ku, Nagoya, Aichi, Japan, **6** Research Center for Ultra-high Voltage Electron Microscopy, Osaka University, Ibaraki, Osaka, Japan

## Abstract

**Background:** Adeno-associated virus (AAV) is well established as a vehicle for *in vivo* gene transfer into the mammalian retina. This virus is promising not only for gene therapy of retinal diseases, but also for *in vivo* functional analysis of retinal genes. Previous reports have shown that AAV can infect various cell types in the developing mouse retina. However, AAV tropism in the developing retina has not yet been examined in detail.

**Methodology/Principal Findings:** We subretinally delivered seven AAV serotypes (AAV2/1, 2/2, 2/5, 2/8, 2/9, 2/10, and 2/11) of AAV-CAG-mCherry into P0 mouse retinas, and quantitatively evaluated the tropisms of each serotype by its infecting degree in retinal cells. After subretinal injection of AAV into postnatal day 0 (P0) mouse retinas, various retinal cell types were efficiently transduced with different AAVs. Photoreceptor cells were efficiently transduced with AAV2/5. Retinal cells, except for bipolar and Müller glial cells, were efficiently transduced with AAV2/9. Horizontal and/or ganglion cells were efficiently transduced with AAV2/1, AAV2/2, AAV2/8, AAV2/9 and AAV2/10. To confirm the usefulness of AAV-mediated gene transfer into the P0 mouse retina, we performed AAV-mediated rescue of the *Cone-rod homeobox* gene knockout (*Crx* KO) mouse, which exhibits an outer segment formation defect, flat electroretinogram (ERG) responses, and photoreceptor degeneration. We injected an AAV expressing *Crx* under the control of the *Crx 2kb* promoter into the neonatal *Crx* KO retina. We showed that AAV mediated-*Crx* expression significantly decreased the abnormalities of the *Crx* KO retina.

**Conclusion/Significance:** In the current study, we report suitable AAV tropisms for delivery into the developing mouse retina. Using AAV2/5 in photoreceptor cells, we demonstrated the possibility of gene replacement for the developmental disorder and subsequent degeneration of retinal photoreceptors caused by the absence of *Crx*.

**Citation:** Watanabe S, Sanuki R, Ueno S, Koyasu T, Hasegawa T, et al. (2013) Tropisms of AAV for Subretinal Delivery to the Neonatal Mouse Retina and Its Application for *In Vivo* Rescue of Developmental Photoreceptor Disorders. PLoS ONE 8(1): e54146. doi:10.1371/journal.pone.0054146

**Editor:** Alfred Lewin, University of Florida, United States of America

**Received:** July 14, 2012; **Accepted:** December 6, 2012; **Published:** January 15, 2013

**Copyright:** © 2013 Watanabe et al. This is an open-access article distributed under the terms of the Creative Commons Attribution License, which permits unrestricted use, distribution, and reproduction in any medium, provided the original author and source are credited.

**Funding:** This work was supported by CREST and from Japan Science and Technology Agency (<http://www.jst.go.jp>), a grant for Molecular Brain Science, Grants-in-Aid for Scientific Research on Priority Areas, and Grant-in-Aid for Scientific Research (B) (#20390087), Young Scientists (B) (#24700360) from the Ministry of Education, Culture, Sports and Technology of Japan (<http://www.jsps.go.jp/>), The Takeda Science Foundation (<http://www.takeda-sci.or.jp/>), The Uehara Memorial Foundation (<http://www.uharazaidan.com/>), Novartis Foundation (#20-10, <http://novartisfound.or.jp/>), The Naito Foundation (<http://www.naito-f.or.jp/>), Senri Life Science Foundation (#S-2144, <http://www.senri-life.or.jp/>), Kato Memorial Bioscience Foundation (<http://www.katoken.or.jp/>), Daiichi-Sankyo Foundation of Life Science; Japanese Retinitis Pigmentosa Society Foundation, and Research Foundation for Opto-Science and Technology (<http://www.jrps.org/>). The funders had no role in study design, data collection and analysis, decision to publish, or preparation of the manuscript.

**Competing Interests:** The authors have declared that no competing interests exist.

\* E-mail: [takahisa.furukawa@protein.osaka-u.ac.jp](mailto:takahisa.furukawa@protein.osaka-u.ac.jp)

## Introduction

Functional analysis of the genes expressed in the mammalian retina is essential for understanding the molecular basis for human retinal development and disease. Recent progress in techniques of comprehensive analysis of gene expression using microarray and next generation sequencing make it possible to obtain many candidate genes that are possibly associated with retinal development and disease [1,2]. Although *in vivo* analysis of candidate genes using transgenic and/or knockout mice is beneficial in revealing the *in vivo* functions of the genes, it is still expensive, time-consuming, and requires a great deal of skill. Therefore, a rapid

and convenient method of *in vivo* gene transfer would be beneficial to the field. To transduce a gene into the mouse retina, *in vivo* electroporation and virus-mediated gene transfer are currently the most available methods. *In vivo* electroporation is a method in which plasmid DNA is incorporated into retinal tissue by high-voltage pulses. This method efficiently transduces DNA into rod photoreceptor cells, but much less efficiently into bipolar, amacrine, and Müller glial cells. Moreover, cone photoreceptor, horizontal, and ganglion cells are barely transduced by *in vivo* electroporation [3]. For virus-mediated transduction, retrovirus, lentivirus, adenovirus, and adeno-associated virus (AAV) have

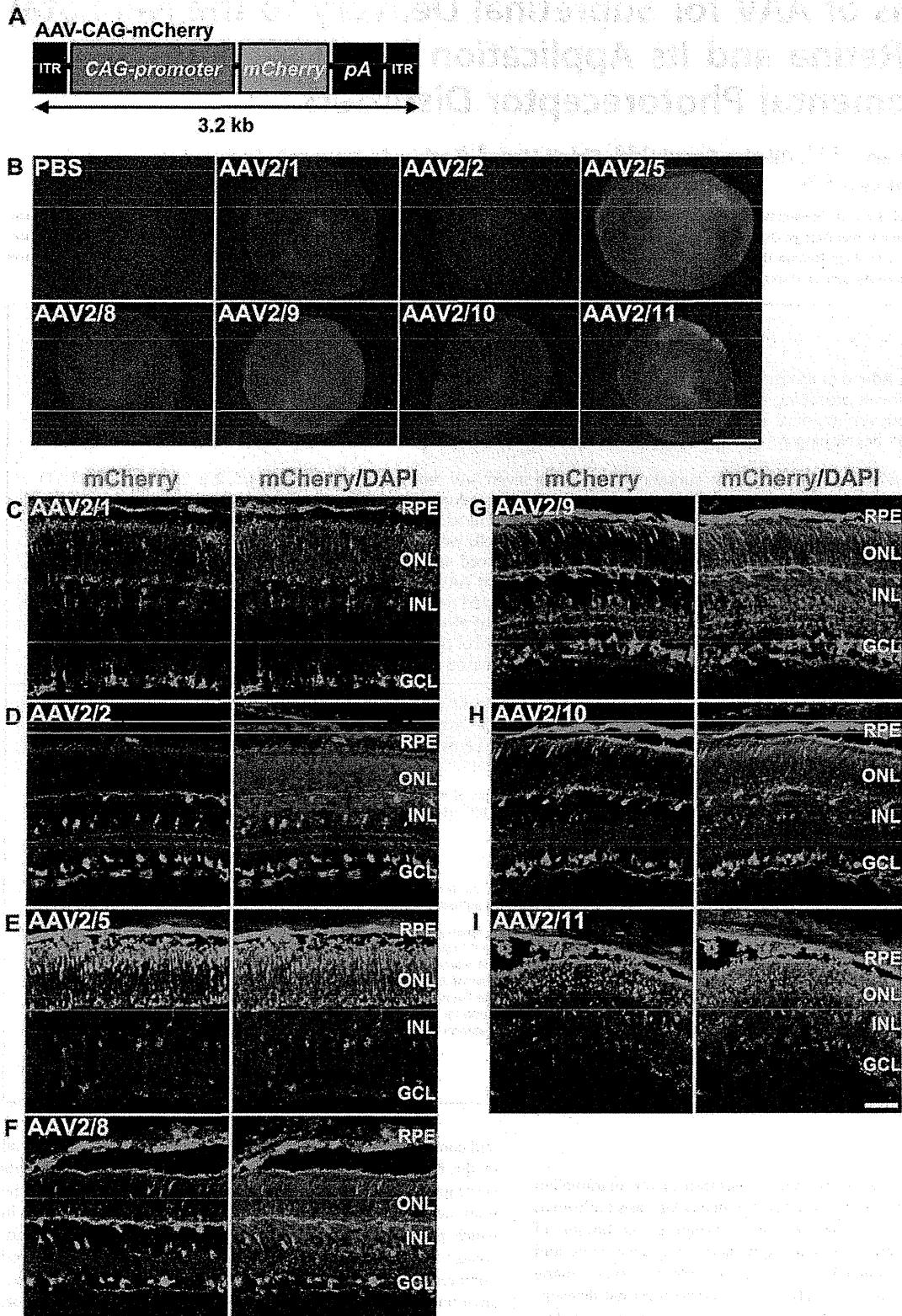


**Figure 1. Tropisms of seven AAV serotypes in the P0 mouse retina.** (A) Schematic diagram of the AAV-CAG-mCherry construct. This AAV drives ubiquitous expression of mCherry under the control of the CAG promoter. (B) Fluorescence images of the distribution of mCherry expression in

whole retinas (photoreceptor-side-up) two weeks after subretinal injection with PBS or one of each of the seven serotypes of AAV-CAG-mCherry. (C–I) Fluorescence images of mCherry expression two weeks after subretinal injection into the P0 mouse retina with AAV2/1- (C), AAV2/2- (D), AAV2/5- (E), AAV2/8- (F), AAV2/9 (G), AAV2/10- (H), and AAV2/11- (I), CAG-mCherry. Scale bar represents 1 mm (B) and 50  $\mu$ m (C–I). ITR: inverted terminal repeat, RPE: retinal pigment epithelium, ONL: outer nuclear layer, INL: inner nuclear layer, GCL: ganglion cell layer.  
doi:10.1371/journal.pone.0054146.g001

been developed as vehicles for retinal gene transfer. In particular, AAV has many advantages for retinal gene transfer, including high transduction efficiency in non-dividing cells, long-term transgene expression, and low-toxicity. AAV is a non-pathogenic parvovirus, which consists of single-stranded DNA covered with capsid proteins. Each AAV serotype is different in the capsid structure, which leads to different tropisms and transduction efficiencies. Twelve serotypes have currently been used as a vehicle for *in vivo* gene transfer (AAV2/1-AAV2/12). AAV tropisms for gene transduction into several murine organs and tissues, including the retina, are different according to developmental stage (neonatal or adult) [4,5]. The previous studies on AAV serotype tropism in subretinal injections into the adult mouse retina revealed that retinal pigment epithelium (RPE) cells are efficiently transduced with AAV2/1, and RPE and photoreceptor cells are efficiently transduced with AAV2/2, AAV2/5 [6,7], and AAV2/8 [7]. However, detailed AAV tropisms for transduction into the developing mouse retina have not been reported.

In the current study, we examined the tropism of seven AAV serotypes (AAV2/1, AAV2/2, AAV2/5, AAV2/8, AAV2/9, AAV2/10, and AAV2/11) by subretinal injection into the P0 mouse retina. We revealed that AAV can transduce encoded genes into various retinal cell types in the developing mouse retina. In addition, to validate the usefulness of AAV-mediated gene transfer into the developing mouse retina, we performed AAV-mediated rescue of *Crx* KO mice. CRX is a transcription factor that is predominantly expressed in photoreceptor cells and is essential for photoreceptor maturation [8,9,10]. We previously reported that *Crx* KO mice exhibit a total lack of outer segment formation, an absence of both scotopic and photopic electroretinograms (ERG), and progressive photoreceptor degeneration [10]. Our AAV-mediated rescue experiment led to a partial restoration of morphological and functional characteristics in the *Crx* KO retina. In humans, the mutations of *Crx* are associated with three forms of retinal degeneration, including cone and rod dystrophy (CORD) [11,12,13], retinitis pigmentosa (RP) [13], and Leber congenital amaurosis (LCA) [13,14], all of which can lead to vision loss. Thus, our results also provide a clue to the suitability of gene therapy for development disorders and degeneration of the retina in humans.

## Results

### Tropisms of Seven AAV Serotypes to the Neonatal Mouse Retina

In order to examine AAV tropisms for subretinal delivery into the P0 mouse retina, we generated AAV2/1-, AAV2/2-, AAV2/5-, AAV2/8-, AAV2/9-, AAV2/10-, and AAV2/11-vectors expressing *mCherry* driven by the ubiquitous promoter, *CAG* promoter (AAV-CAG-mCherry) (Fig. 1A). We selected six serotypes (AAV2/1, 2/2, 2/5, 2/8, 2/9, 2/10), because they are known to be infectious to the mammalian central nervous system (Gene therapy program at university of Pennsylvania (<http://www.med.upenn.edu/gtp/>)), and have previously been examined for tropisms for subretinal or intravitreal transduction into the adult mouse retina [6,7,15]. Since the AAV2/11 serotype was recently discovered [16], we also tested this serotype in addition to the other six. Each of the seven tested serotypes of AAV was subretinally injected into the P0 mouse retina. We harvested the

injected retinas at 14 days after injection, P14, when all retinal cells had finished generating (Fig. 1B–I). We observed that mCherry expression was evenly distributed in the retinas injected with each of the seven serotypes of AAV-CAG-mCherry (Fig. 1B). AAV2/5- and AAV2/9-injected retinas showed intense mCherry signals throughout, and AAV2/2-, AAV2/8-, and AAV2/10-injected retinas showed substantial mCherry signals (Fig. 1B). Photoreceptor cells were efficiently transduced with AAV2/1, AAV2/5, AAV2/9, and AAV2/11 (Fig. 1C, E, G, I). In particular, the AAV2/5-injected retina showed mCherry expression predominantly in photoreceptor cells (Fig. 1E). The AAV2/9-injected retina showed mCherry expression throughout the retina (Fig. 1G). Horizontal cells were efficiently transduced with AAV2/1, AAV2/2, AAV2/8, AAV2/9, and AAV2/10 (Fig. 1C, D, F–H). Müller glial cells were efficiently transduced with AAV2/1 (Fig. 1C). In addition, the RPE was well transduced with all serotypes (Fig. 1C–I).

### Infection Efficiencies of Seven AAV Serotypes

To quantitatively assess the tropism of seven AAV serotypes in the mouse retina, we measured the infection efficiencies for each retinal cell type. Infection efficiency is calculated by the percentage of cells expressing mCherry out of retinal cell-specific marker-positive cells (Fig. 2A). Photoreceptor and horizontal cells were efficiently transduced with AAV2/1 (Fig. 2B, Rod:  $65.5 \pm 3.9\%$  in the middle area, Cone:  $80.8 \pm 4.5\%$  and horizontal:  $55.6 \pm 9.2\%$ ). The AAV2/1-injected retinas also exhibited the highest efficiency for Müller glial cells among seven serotypes (Fig. 2B,  $47.9 \pm 5.8\%$ ). AAV2/2 and AAV2/8 showed similar transduction patterns with each other, and horizontal and ganglion cells were transduced mainly with these serotypes (Fig. 2C, E, horizontal cells:  $78.2 \pm 3.2\%$  and  $76.6 \pm 12.2\%$  respectively; ganglion cells:  $46.9 \pm 9.4\%$  and  $40.7 \pm 0.1\%$  respectively). AAV2/5 displayed the highest infection efficiency for rod and cone photoreceptor cells (Fig. 2D, rod:  $84.5 \pm 10.3\%$  in middle area and cone;  $92.2 \pm 4.4\%$ ). Retinal cells except for bipolar and Müller glial cells were efficiently infected with AAV2/9, and infection efficiencies of AAV2/9 for horizontal and ganglion cells were the highest among seven serotypes (Fig. 2F, horizontal;  $92.7 \pm 0.6\%$  and ganglion;  $82.0 \pm 0.1\%$ ). AAV2/9 showed the highest efficiency in amacrine cells (Fig. 2F,  $34.8 \pm 3.2\%$ ). AAV 2/10 efficiently targeted horizontal and ganglion cells (Fig. 2G, horizontal cells:  $81.0 \pm 9.9\%$  and ganglion cells:  $72.1 \pm 0.1\%$ ). AAV2/11 showed efficient infection in photoreceptor cells (Fig. 2H, rod:  $70.0 \pm 8.6\%$  in middle area and cone:  $56.3 \pm 8.2\%$ ). Bipolar cells exhibited very low efficiency or no infection detected among all analyzed serotypes (Fig. 2B–H).

### AAV-mediated Rescue Experiment for the *Crx* KO Retina

To validate the usefulness of AAV-mediated gene transfer into the developing mouse retina, we performed an AAV-mediated rescue experiment for the *Crx* KO mice. CRX is a transcription factor which plays a crucial role in photoreceptor maturation through photoreceptor gene transactivation [1,8,9,10]. We generated an AAV2/5 vector expressing Flag-tagged *Crx* cDNA under the control of the *Crx* 2kb promoter to drive specific expression in photoreceptor cells (AAV2/5-Crx2kb-Flag-Crx = AAV-Crx) [17,18] (Fig. 3A). We injected AAV-Crx subretinally into *Crx*

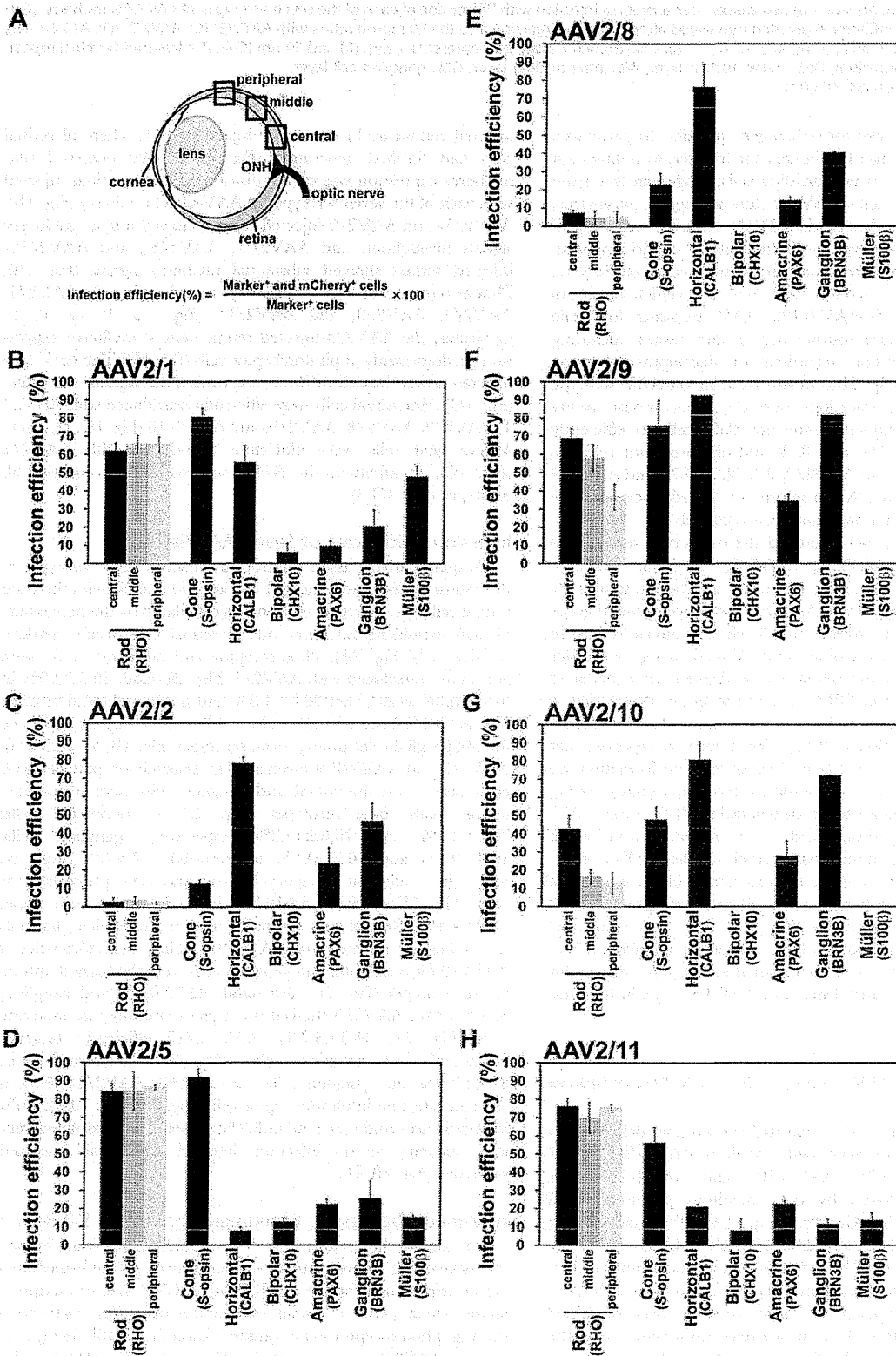


**Figure 2. Infection efficiencies of seven AAV serotypes in each retinal cell type.** (A) Schematic diagram of quantification method of infection efficiency. Two weeks after subretinal injection, the retinas were immunostained with antibodies of retinal cell type-specific markers (Rod:

RHODOPSIN (RHO), Cone: S-OPSIN, Horizontal: CALB1, Bipolar: CHX10, Amacrine: PAX6, Ganglion: BRN3B, Müller: S100 $\beta$ ). According to retinal cell types, the numbers of marker-positive and marker/mCherry double-positive cells were counted for calculation of infection efficiency ( $n=3$  from three different mice). Cells were counted in the central area of the retina for calculating the infection efficiencies of cone photoreceptor, bipolar, and Müller glial cells, and in the central, middle and peripheral areas of the retina for calculating the infection efficiencies of rod photoreceptor and amacrine cells. Infection efficiency was calculated using the formula indicated in Figure 2A. (B–H) Infection efficiencies of AAV2/1- (B), AAV2/2- (C), AAV2/5- (D), AAV2/8- (E), AAV2/9- (F), AAV2/10- (G), and AAV2/11- (H), CAG-mCherry. Error bar represents the SD from the means of three retinas. ONH: optic nerve head.

doi:10.1371/journal.pone.0054146.g002

KO retinas at P0. To confirm the *Flag-Crx* expression in the retina, we performed an RT-qPCR analysis using RNA from the whole retina at three weeks after injection. We observed significant expression of *Flag-Crx* mRNA in the *Crx* KO retinas treated with AAV-Crx (Fig. 3B). We further analyzed FLAG-CRX expression in control and AAV-Crx treated retinas by western blotting using an anti-FLAG antibody. We detected a 38 kDa FLAG-CRX band in the AAV-treated *Crx* KO retinal lysates (Fig. 3C). To determine whether FLAG-CRX is expressed in photoreceptor cells, we performed an immunostaining of the control *Crx* KO and AAV-Crx-injected *Crx* KO retinas with the anti-FLAG antibody. FLAG signals were predominantly detected in photoreceptor cells in AAV-Crx-treated *Crx* KO retinas (Fig. 3D). Non-specific signals were also detected in the RPE and blood vessels in the INL in both control and AAV-Crx-treated *Crx* KO retinas. This is very likely due to autofluorescence from the RPE and to the reaction of the anti-mouse secondary antibody to endogenous mouse antibodies in the blood vessels (Fig. 3D). AAV-Crx-mediated FLAG-CRX expression was widely distributed throughout the AAV-Crx-treated *Crx* KO retinas (Fig. 3E, F).

The expression profiling of the *Crx* KO retina using microarray identified a number of photoreceptor genes down-regulated in the *Crx* KO retina involved in phototransduction, ciliary function, transcriptional regulation of photoreceptor genes, and synaptic development [10,19]. In humans, mutations of some of these gene homologues cause retinal diseases, including retinal degeneration, color blindness and night blindness (RetNet: <https://sph.uth.tmc.edu/retnet/>). Down-regulation of these genes is likely to underlie the phenotypes of the *Crx* KO retina. Thus, we performed an expression analysis of photoreceptor genes, which are down-regulated in the *Crx* KO retina and related to human retinal diseases, in AAV-Crx-treated *Crx* KO retinas. We performed RT-qPCR analyses on the following eleven genes: *Rhodopsin* (phototransduction, RP and Congenital stationary night blindness (CSNB)), *Gnat1* (phototransduction, CSNB), *S-opsin*, *M-opsin* (phototransduction, color blindness), *Pde6g* (phototransduction, RP), *Slc24a1* (phototransduction, CSNB), *Rdh12* (visual cycle, LCA and RP), *Rpgrip1* (ciliary function, LCA and CORD), *Nrl* (transcription regulation, RP), *Cabp4* (synaptic function, CSNB, LCA), and *Fscn2* (Cytoskeleton regulation, RP and macular dystrophy). In AAV-Crx-treated *Crx* KO retinas, we observed substantial up-regulation of *S-opsin*, *M-opsin*, and *Fscn2* (Fig. 3I, J, Q) and modest up-regulation of *Rhodopsin*, *Gnat1*, *Pde6g*, *Slc24a1*, *Rdh12*, *Rpgrip1*, *Nrl*, and *Cabp4* (Fig. 3G, H, K–P).

#### Immunohistochemistry of *Crx* KO Retinas Treated with AAV-Crx

We further analyzed the expression of RHODOPSIN, GNAT1, S-OPSIN, and M-OPSIN in AAV-Crx-treated *Crx* KO retinas by immunostaining. The RHODOPSIN protein level was slightly increased in AAV-Crx-injected *Crx* KO retinas (Fig. 4A–D), while GNAT1 signals were markedly increased (Fig. 4E–H). Similarly, S-OPSIN and M-OPSIN signals were markedly increased (Fig. 4I–P). Consistent with the results of the RT-qPCR analysis shown in Figure 3G–Q, the levels of these molecules also increased in AAV-

Crx-treated *Crx* KO retinas. In addition, GNAT1, S-OPSIN, and M-OPSIN signals appeared to be localized in outer segments in AAV-Crx-injected *Crx* KO retinas (Fig. 4E–P). RHODOPSIN and GNAT1 are localized in the rod outer segment and S-OPSIN and M-OPSIN are localized in the cone outer segment. The *Crx* KO retina lacks outer segment formation [10,20]. This immunohistochemical data suggests that the defect of outer segment formation in the *Crx* KO retina was partially restored by the subretinal injection of AAV-Crx into *Crx* KO retinas.

We further examined the morphology of the outer segment in the control *Crx* KO and AAV-Crx-injected *Crx* KO retinas in detail by transmission electron microscopy at fifteen weeks after AAV treatment (Fig. 4Q–S). We observed no photoreceptor cells in control retinas because of severe photoreceptor degeneration in the *Crx* KO retina (Fig. 4Q). In contrast, outer segments containing disk lamina were observed in AAV-Crx-injected *Crx* KO retinas (Fig. 4R, S). These data showed that the subretinal delivery of AAV-Crx into P0 *Crx* KO retinas partially restored outer segment formation in the *Crx* KO mice.

#### The Improvement of Retinal Function in the *Crx* KO Retina Treated with AAV-Crx

To evaluate the effect of the AAV-Crx injection on retinal function, we performed electroretinogram (ERG) recordings. *Crx* KO mice exhibit flat scotopic and photopic ERG responses at P30, resulting from the defect of formation of outer segments and considerable loss of phototransduction molecules in the *Crx* KO mice [10]. At 6 and 15 weeks after AAV treatment, we measured ERG responses from three control and three AAV-Crx-treated eyes. The mice used for ERG recordings were independently prepared between the two time points. We first tried to record scotopic ERG responses from the AAV-treated mouse eyes in a conventional way [21,22], but no positive response was detected. Therefore, we then measured photopic ERG responses with one hundred stroboscopic flashes of 1.0 log cd-s/m<sup>2</sup>. The ERG responses obtained under these conditions majorly reflect cone photoreceptor functions. Consistent with our previous observation [10], all of the control eyes exhibited completely flat responses at both 6 and 15 weeks after AAV treatment (Fig. 5A top, Table 1). In contrast, two of three AAV-Crx-treated eyes showed significant photopic a- and b-waves at both 6 and 15 weeks after AAV treatment (Fig. 5A bottom, Table 1). One of the AAV-Crx-treated *Crx* KO mice did not show a detectable ERG photopic response. Although this mouse eye widely expressed FLAG-CRX, the eye was much smaller than the other two mouse eyes and was severely damaged histologically (data not shown), probably due to subretinal injection damage, resulting in physiological dysfunction. This result shows that the subretinal injection of AAV-Crx into *Crx* KO retinas partially restored the physiological function of *Crx* KO photoreceptor cells.

Progressive photoreceptor degeneration is also observed in the *Crx* KO mice [10]. We examined photoreceptor degeneration in the retinas fifteen weeks after AAV treatment by immunostaining using an anti-FLAG antibody (Fig. 5B). Although there was substantial photoreceptor cell death in both control and AAV-Crx-

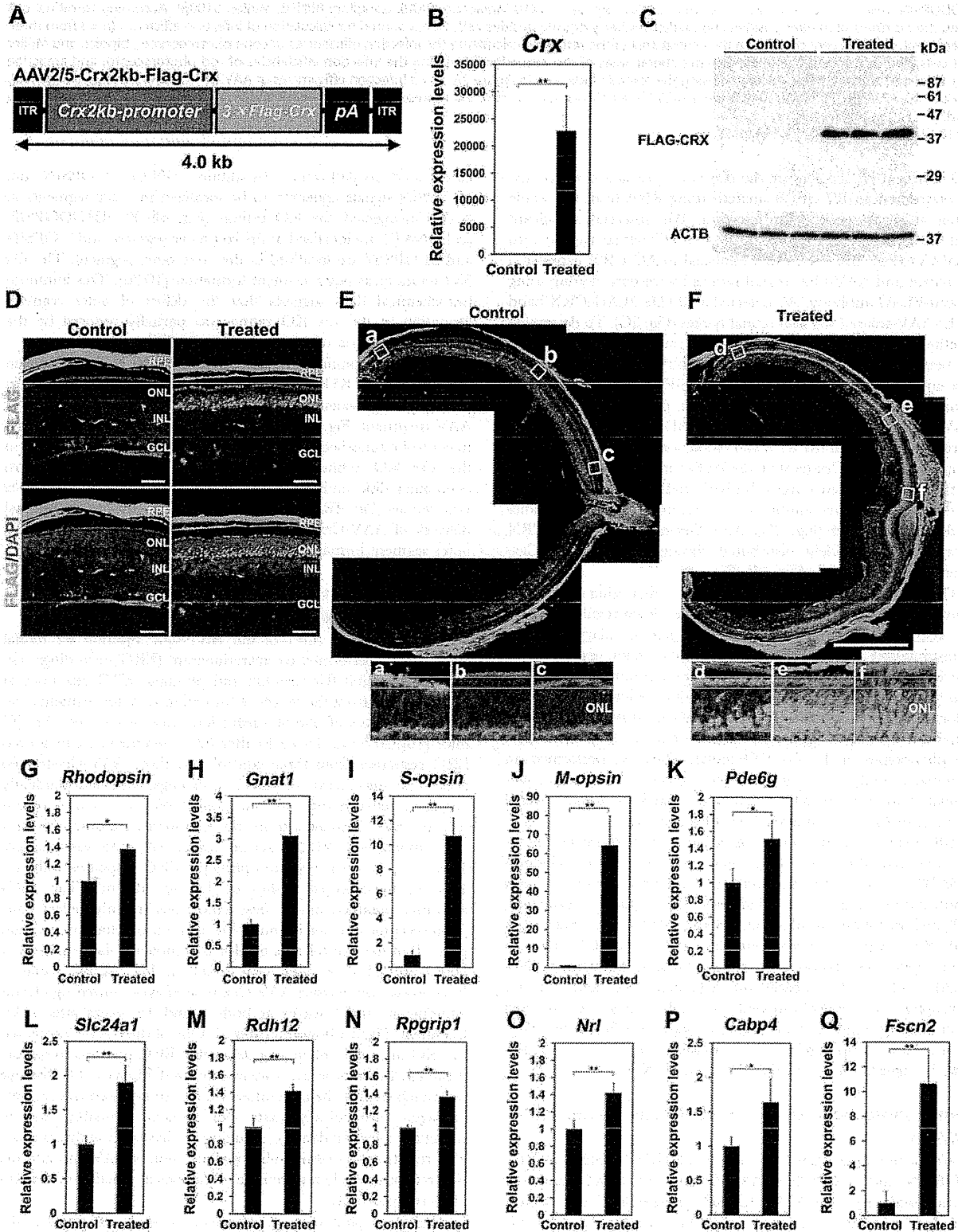


**Figure 3. Gene expression analysis of the *Crx* KO retina treated with AAV-Crx.** (A) Schematic diagram of the AAV2/5-Crx2kb-Flag-Crx construct. (B) Expression analysis of *Crx* by RT-qPCR using RNA isolated from control and AAV-treated *Crx* KO retinas (Control *Crx* KO retinas:  $n=3$  from three different mice and AAV-treated *Crx* KO retinas:  $n=4$  from four different mice). (C) Western blot analysis of FLAG-CRX using control and



AAV-treated *Crx* KO retinas from three different mice respectively. An anti-FLAG antibody was used to detect FLAG-CRX. ACTB ( $\beta$ -actin) was used as a loading control. (D–F) Immunostaining of the *Crx* KO retinas treated with AAV-Crx or PBS using an anti-FLAG antibody. The distribution of FLAG-CRX expression in control and AAV-Crx treated *Crx* KO retinas (E, F). Enlarged images in white boxes (a–c and d–f) in Figure 3E and F, respectively. Scale bar represents 50  $\mu$ m (D) and 1 mm (E, F). (G–Q) Expression analyses of eleven genes related to human retinal diseases three weeks after treatment (Control *Crx* KO retinas:  $n=3$  from three different mice and AAV-treated *Crx* KO retinas:  $n=4$  from four different mice). *Rhodopsin* (G), *Gnat1* (H), *S-opsin* (I), *M-opsin* (J), *Pde6g* (K), *Slc24a1* (L), *Rdh12* (M), *Rpgrip1* (N), *Nrl* (O), *Cabp4* (P), and *Fscn2* (Q). Control retinas were injected with PBS (Vehicle). *Rpl4* was used for normalization. Primers for qPCR were listed in Table S1. Error bar represents the SD from the means of three control retinas and four treated retinas. \*\* $p<0.01$ , \* $p<0.05$ . ITR: inverted terminal repeat, RPE: retinal pigment epithelium, ONL: outer nuclear layer, INL: inner nuclear layer, GCL: ganglion cell layer.  
doi:10.1371/journal.pone.0054146.g003

treated *Crx* KO retinas, AAV-Crx-treated *Crx* KO retinas had a thicker outer nuclear layer than that of control retinas (Fig. 5B top panels). Remarkably, most of the surviving photoreceptor cells in AAV-Crx-treated *Crx* KO retinas expressed FLAG-CRX (Fig. 5B bottom panels). This observation suggests that photoreceptor cells without FLAG-CRX expression died and that AAV-Crx inhibited photoreceptor cell death in the *Crx* KO retinas. To confirm this result, we performed immunostaining with an anti-active-caspase-3 antibody, an apoptosis marker, three weeks after AAV treatment (Fig. 5C, D). We observed a significant reduction of apoptotic cell numbers in AAV-Crx-treated *Crx* KO retinas (Fig. 5C, D). These results show that subretinal injection of AAV-Crx prevented photoreceptor cell death to some extent in the *Crx* KO retina.

## Discussion

The main goal of this study is to establish a method for AAV-mediated retinal gene transfer into developing retinas for *in vivo* analysis of retinal genes and to apply the method to the rescue of retinal degeneration. Through the transduction of AAV-CAG-mCherry into the developing mouse retina, we showed that various retinal cell types were transduced differently with each of seven serotypes of AAV. We quantitatively analyzed infection efficiencies of these AAV serotypes. In addition, we demonstrated the usefulness of AAV transduction into the developing mouse retina for the rescue of the retinal degeneration of *Crx* KO mice. These results will be useful to researchers who perform *in vivo* analysis of retinal genes using AAV.

We subretinally injected seven serotypes of AAV into the P0 mouse retina. We chose P0, because the retina at this stage is still developing and amenable to surgical treatment by subretinal injection. Serotypes AAV2/5 and AAV2/9 exhibited remarkable and efficient infection. Photoreceptor cells were selectively and efficiently transduced with AAV2/5. Retinal cells, except for Müller glial cells and bipolar cells, were efficiently transduced with AAV2/9. We observed efficient transduction into horizontal and/or ganglion cells with AAV2/1, AAV2/2, AAV2/8, AAV2/9 and AAV2/10. These data suggests that *in vivo* gene transfer by subretinal injection of AAV into the mouse retina enables us to analyze gene function in retinal cell types that are difficult or impossible to transduce by *in vivo* electroporation (cone photoreceptor, horizontal, and ganglion cells) [3]. To perform an analysis specifically in a certain cell type in the retina, a cell type-specific promoter of relatively short length for each cell type will need to be developed in the future.

In the current study, the infection efficiencies of AAV into bipolar and Müller glial cells were low in all tested serotypes, although AAV2/1 efficiently targeted Müller glial cells. These two retinal cells undergo differentiation at the latest stages during development [21]. In contrast, retinal cells, which are generated at embryonic stages or at early postnatal stages (photoreceptor, horizontal, amacrine and ganglion cells), were transduced with all analyzed serotypes. These results suggest that the AAV serotypes tested in this study are more infectious to differentiated retinal cells

than to retinal progenitor or differentiating cells. Since more than 100 AAV serotypes have been isolated [22], AAV serotypes which are capable of efficiently infecting bipolar and Müller glial cells may be found in the future. Our observations on AAV tropism in the developing retina in the current study may expand the application of AAV for *in vivo* transduction to retinal cell types, such as cone photoreceptors, horizontal cells, and ganglion cells, which are barely transduced by *in vivo* electroporation. The AAV tropisms shown in the current study were different from those for the adult mouse retina in previous reports. In subretinal transduction into the adult retina AAV2/1 mainly targets RPE cells, and AAV2/2, 2/5, and 2/8 mainly target both RPE and photoreceptor cells [6,7]. However, based on our results using P0 mice, each AAV serotype targeted several retinal cell types. This observation is consistent with the results reported by Surace *et al.* [5], in which they showed the difference of tropisms for transduction into fetal, neonatal and adult retinas using AAV2/1-, 2/2-, and 2/5-CMV-EGFP. There are two possible explanations for the shift of AAV tropism between the developing retina and the mature retina. The first is that the expression or abundance of AAV receptors in host retinal cells may change during retinal development. The second is that injected virus particles may more easily diffuse across the retina due to the smaller size of the P0 retina and dynamic cell migration during retinal development. The differences of AAV tropisms between neonatal and adult mice are also observed in the aorta, liver and kidney [4]. This suggests that the time point of transduction of an AAV vector during development is important to appropriately perform gene transfer to a cell type of interest.

We attached the *Crx 2kb* promoter to the AAV vector for the rescue experiment on the *Crx* KO retina. We previously reported that this promoter directs specific gene expression in developing and mature rod and cone photoreceptor cells [17,18]. Expression analysis by RT-qPCR and immunohistochemistry showed improved expression of both rod-specific genes (*Rhodopsin* and *Gnat1*) and cone-specific genes (*S-opsin* and *M-opsin*) in AAV-Crx-treated *Crx* KO retinas (Fig. 3G–Q and 4A–P). This indicates that the *Crx 2kb* promoter successfully drove the *Crx* expression in both rod and cone photoreceptor cells. Thus the *Crx 2kb* promoter can be used with AAV to drive expression specifically in photoreceptor cells.

AAV-Crx modestly but significantly improved the photopic ERG responses, but we were not able to detect scotopic ERG responses in AAV-treated eyes. In order to detect relatively weak ERG responses in AAV-Crx-treated *Crx* KO eyes, we stimulated the mouse eyes with one hundred stroboscopic flashes (1.0 log cd $\cdot$ s/m $^2$ ). However, under these conditions, it is very difficult to measure scotopic ERG responses because the intermittently repeated flashing lights abrogate the dark adaptation that is necessary for scotopic ERG recordings. Because of such technical difficulties, we were not practically able to measure scotopic ERG responses in our current study. AAV-Crx also partially restored outer segment formation in the *Crx* KO mice. This result not only confirms that AAV transduction into the P0 retina is a useful method for *in vivo* retinal gene transfer but also suggests that gene

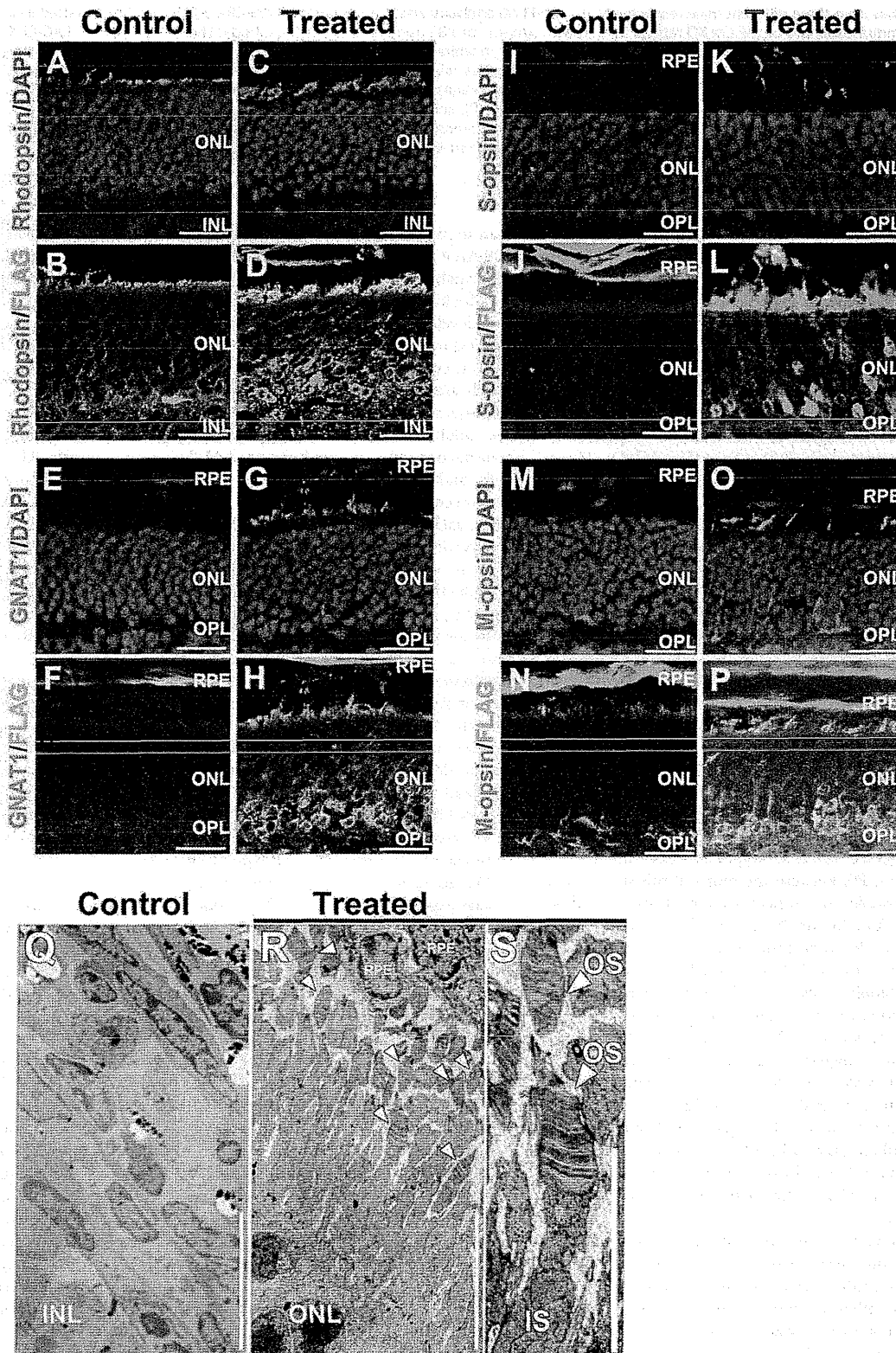


**Figure 4. Histological analyses of the *Crx* KO retina transduced with AAV-Crx.** (A–P) Immunostaining of the *Crx* KO retinas three weeks after AAV-Crx treatment with outer segment makers of rod photoreceptor (A–H) and cone photoreceptor cells (I–P). Scale bars represent 20  $\mu$ m (A–P). (Q–



S) Transmission electron microscopy analysis of retinas fifteen weeks after AAV-Crx treatment. (Q and R) In control retinas, no photoreceptor cell was observed (Q). In AAV-Crx-treated retinas, some outer segment structures were observed (R). (S) An enlarged image of outer segments in AAV-Crx-treated retinas. Arrowheads indicate outer segment containing disk lamina. Scale bars represent 7.5  $\mu\text{m}$  (Q and R) and 5  $\mu\text{m}$  (S). RPE: retinal pigment epithelium, ONL: outer nuclear layer, OPL: outer plexiform layer, INL: inner nuclear layer, GCL: ganglion cell layer. OS: outer segment, IS: inner segment.

doi:10.1371/journal.pone.0054146.g004

therapy for human retinal diseases caused by *Crx* mutations is possible. In addition, this is the first report on AAV-mediated rescue for mice with mutations of a transcription factor regulating photoreceptor development and related to human photoreceptor degeneration. *Nrl*, *Nr2e3*, and *Otx2* also play crucial roles in photoreceptor development through transcriptional regulation of photoreceptor genes [1,23,24,25]. The mutations of these genes in humans are associated with several types of retinal degeneration (RetNet: <https://sph.uth.tmc.edu/retnet/home.htm>). Our current result suggests that human retinal degenerations caused by the mutations in these transcription factors can be restored by AAV-mediated gene therapy. This possibility will be examined by AAV-mediated rescue of mice with these gene mutations in the future.

## Materials and Methods

### Animals

For the evaluation of the tropism of AAVs *in vivo*, we used ICR mice (Charles River). The *Crx* KO mice were generated as described in our previous study [10]. All procedures conformed to the ARVO statement for the Use of Animals in Ophthalmic and Vision Research, and these procedures were approved by the Institutional Safety Committee on Recombinant DNA Experiments and the Animal Research Committee of Osaka Bioscience Institute (approval ID 10-401) and Institute for Protein Research, Osaka University (approval ID 24-05-0). Mice were housed in a temperature-controlled room with a 12-hour light/dark cycle. Fresh water and rodent diet were available at all times.

### Plasmid Constructs

For the production of AAV-CAG-mCherry and AAV2/5-Crx2kb-Flag-Crx, we constructed *pAAV-CAG-mCherry* and *pAAV-Crx2kb-Flag-Crx*, respectively. The *CAG* promoter used in this study was previously described [26]. To produce *pAAV-CAG-mCherry*, we initially constructed *pCAGGS-mCherry*. We cut *pAAV-U6-shLhx2-CMV-mCherry* [27] with *NheI* and *NotI* and inserted the *mCherry* fragment into *pCAGGS* digested *EcoRI* and *NotI* using a *NheI/EcoRI* linker. Finally, to produce *pAAV-CAG-mCherry*, we obtained the *CAG-mCherry* fragment by cutting *pCAGGS-mCherry* with *SallI* and *BglII*, and inserted its fragment into *pAAV-IRES-hrGFP* (Agilent technologies) digested with *NotI* and *BglII* using a *NotI/SallI* linker DNA. To produce *pAAV-Crx2kb-Flag-Crx*, we initially constructed *pCRX(2K)-Flag-Crx- $\beta$ gal* [17]. The *Flag-mouseCrx* fragment was obtained by cutting *pcDNA3-Flag-Crx* [28] with *XhoI* and *XbaI*. We inserted it into *pCRX(2K)- $\beta$ gal* digested with *KpnI* and *NheI* using an *XhoI/SallI* linker DNA and obtained *pCRX(2K)-Flag-Crx- $\beta$ gal*. We next constructed *pCRII-bluntI-Crx2kb-Flag-Crx*. We first obtained the *Crx2kb-Flag-Crx* fragment by cutting *pCRX(2K)-Flag-Crx- $\beta$ gal* with *SallI* and *XhoI*. We inserted it into *pCRII-bluntI* digested with *XhoI*, and obtained *pCRII-bluntI-Crx2kb-Flag-Crx*. Finally, to produce *pAAV-Crx2kb-Flag-Crx*, we cut *pCRII-bluntI-Crx2kb-Flag-Crx* with *NotI* and *XhoI*, and inserted its fragment using a *NotI/BglIII* linker into *pAAV-IRES-hrGFP* (Agilent technologies) digested with *NotI* and *BglIII*.

### AAV Production

AAV was produced by triple transfection of an AAV vector plasmid, an adenovirus helper plasmid, and an AAV helper plasmid (*pAAV2/1*, *pAAV-RC* [Agilent technologies], *pXR5*, *pAAV2/8*, *pAAV2/9*, *pAAV2/rh10*, and *pEEV2/11*) into AAV-293 cells by the calcium phosphate method. The cells were harvested at 72 hours after transfection, and lysed by four freeze-and-thaw cycles. The supernatant was collected by centrifugation, and treated with Benzonase nuclease (Novagen) to eliminate cellular DNA/RNA and excess plasmid DNAs. This virus preparation was used for subretinal administration. A titer of each AAV (in vector genomes (VG)/mL) was determined by qPCR using SYBR GreenER Q-PCR Super Mix (Invitrogen) and Thermal Cycler Dice Real Time System MRQ TP870 (Takara). The primers used for AAV titrations are listed in Table S1. The titers of all serotypes of AAV-CAG-mCherry used in this study were adjusted to approximately  $2 \times 10^{12}$  VG/mL. The titer of AAV2/5-Crx2kb-Flag-Crx used in the *Crx* KO rescue experiment is  $2.6 \times 10^{12}$  VG/mL.

### Subretinal Injection

Subretinal injection of AAV was performed as described elsewhere [3,29]. P0 mice were anesthetized by chilling on ice, the eye was opened by cutting along the fused junctional epithelium where the two eyelids come together, and a small incision was made with a 30-gauge needle in the sclera near the junction with the cornea. 0.4  $\mu\text{L}$  of an AAV preparation was injected into the subretinal space through the incision using an Ito micro syringe (Ito Corporation) with a 33-gauge blunt-ended needle under a dissecting microscope. Fast Green dye was added to AAV preparations at a final concentration of 0.1% as a tracer to confirm that the AAV preparations were injected into the subretinal space [29]. For histological analyses, we only used retinas in which the dye in the AAV preparation was confirmed to be evenly distributed and which were without severe damage caused by the injection process.

### Immunostaining

For immunohistochemistry, 14  $\mu\text{m}$  thick retina sections were washed twice in phosphate-buffered saline (PBS), and permeabilized with 0.1% Triton X-100 (wt/vol) in PBS, then incubated with PBS containing 4% donkey serum (vol/vol) for 1 h to block samples. The samples were incubated with a primary antibody at 4°C overnight. After washing with PBS, these samples were incubated with secondary antibodies at 25°C for 1 hour. In the current study, we also used the following primary antibodies: anti-RHODOPSIN antibody (1:10000, O4886, Sigma) as a rod photoreceptor cell marker, anti-S-OPSIN antibody (1:500, sc-14363, Santa Cruz) as a cone photoreceptor cell marker, anti-CALB1 antibody (1:1000, PC253L, Sigma) as a horizontal cell marker, anti-CHX10 antibody (1:200, MBL) as a bipolar cell marker, anti-PAX6 antibody (1:100, DSHB) as an amacrine cell marker, anti-BRN3B antibody (1:100, sc-6026, Santa Cruz) as a ganglion cell maker, anti-S100 $\beta$  antibody (1:100, S-2532, Sigma) as Müller glial cell marker, anti-GNAT1 antibody (1:3000, sc-389, Santa Cruz), anti-M-OPSIN antibody (1:500, AB5402, Chemicon), and anti-FLAG antibody (1:1000, F1804, Sigma). The

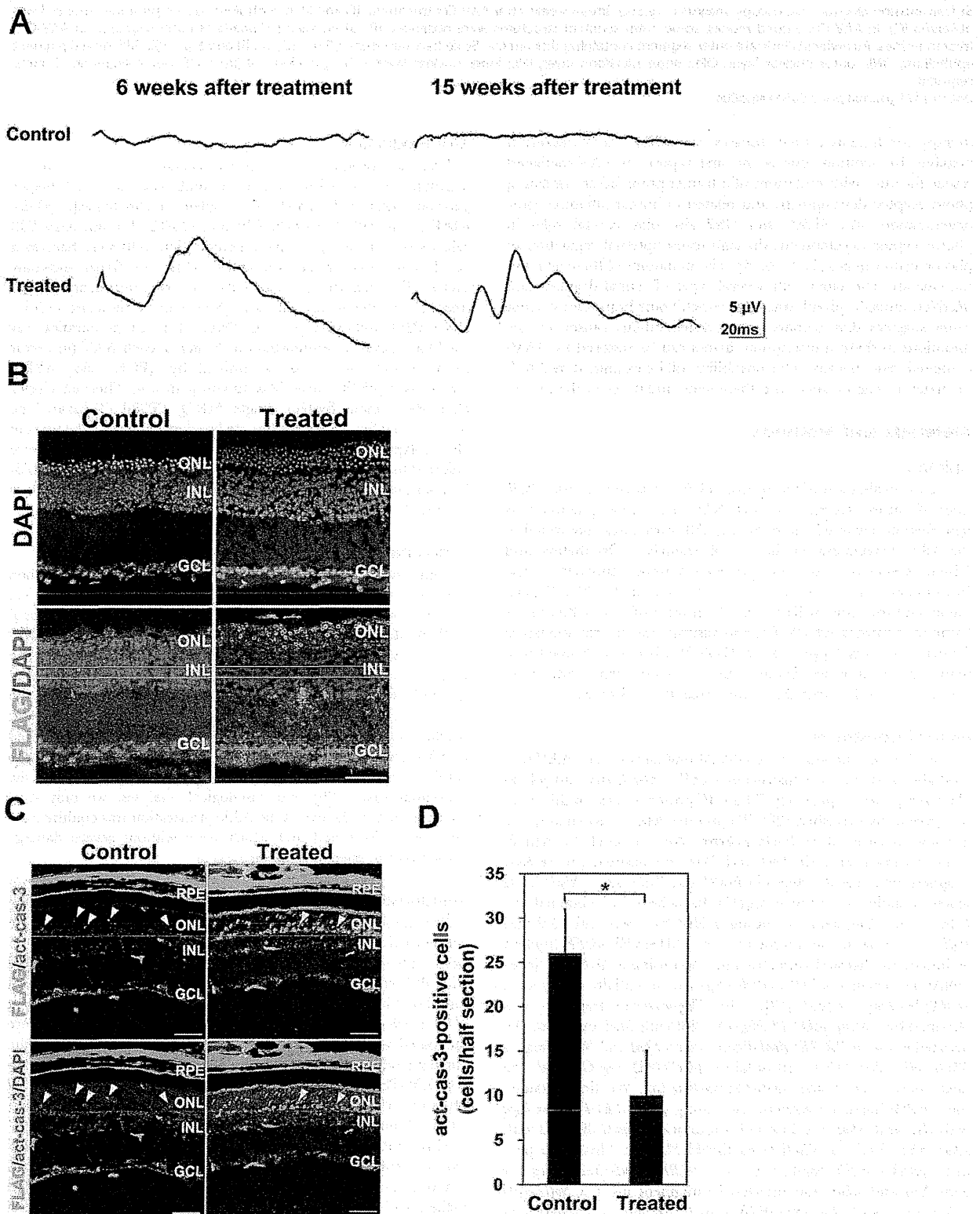


**Figure 5. Restoration of function and morphology in the *Crx* KO retina treated with AAV-*Crx*.** (A) Representative ERGs recorded at six and fifteen weeks after AAV-*Crx* treatment. ERG responses averaged from one hundred 1.0 log cd-s/m<sup>2</sup> stimuli. The mice used for ERG recordings were independently prepared between the two time points. At both six and fifteen weeks after AAV treatment, all three of the control eyes from different

mice showed no ERG response, while two of the three treated eyes from different mice showed significant responses. (B) Immunostaining of FLAG-CRX in the retinas at fifteen weeks after AAV-Crx treatment. (C and D) Immunostaining of active-caspase-3 and FLAG-CRX in Crx KO retinas three weeks after AAV-Crx treatment (C). The number of active-caspase-3-positive cells (D, Control retinas:  $n=3$  from three different mice and AAV-treated Crx KO retinas:  $n=4$  from four different mice). Arrowheads indicate active-caspase-3-positive cells. Scale bar represents 50  $\mu\text{m}$ . Error bar represents the SD from the means of three control retinas and four treated retinas. \* $p<0.05$ . RPE: retinal pigment epithelium, ONL: outer nuclear layer, INL: inner nuclear layer, GCL: ganglion cell layer.  
doi:10.1371/journal.pone.0054146.g005

following secondary antibodies were also used: Alexa Fluor 488-conjugated anti-mouse IgG (1:300, A11001, Invitrogen), Alexa Fluor 488-conjugated anti-rabbit IgG (1:300, A11008, Invitrogen), Alexa Fluor 488-conjugated anti-goat IgG (1:300, A11055, Invitrogen), Cy3-conjugated anti-mouse IgG (1:300, 715-165-150, Jackson), and Cy3-conjugated anti-rabbit IgG (1:300, 705-165-147, Jackson). For immunostaining of the whole retina, each retina was gently peeled off from the sclera, rinsed in PBS, and fixed with 4% paraformaldehyde (wt/vol) in PBS for 1.5 h. The retinas were permeabilized by incubation in 0.1% Triton X-100 in PBS (PBST) for 30 min. After washing in PBST, samples were blocked with 4% donkey serum in PBST for 1 h. The retinas were then immunostained with primary antibodies against mCherry (1:1000, 632496, Clontech) at 4°C overnight. After washing in PBST, reactions with a Cy3-conjugated anti-rabbit IgG secondary antibody were performed overnight at 4°C.

### Quantification of Infection Efficiency

AAV-CAG-mCherry-injected retinas were co-immunostained with cell type-specific markers for each retinal cell shown above and an anti-mCherry antibody. We counted the number of marker-positive cells and marker/mCherry double-positive cells according to cell types for the calculation of infection efficiencies. We used high-resolution confocal images of retinal sections along the z-axis (2.0  $\mu\text{m}$ ) taken with the LSM 700 (Zeiss, 20 $\times$  or 40 $\times$  objectives) to count cell numbers and measure infection efficiencies for rod and cone photoreceptor, bipolar, Müller glial, and amacrine cells. Since horizontal and ganglion cells in the confocal images (20 $\times$ ) are small in number (<10 cells), it is very difficult to

accurately calculate the infection efficiencies of these cell types in contrast to other cell types. Thus, we counted the whole cell numbers seen through a fluorescence microscope for calculating the infection efficiencies of these cell types. We used three retinas from three different mice and counted 100–200 rod photoreceptor and amacrine cell marker-positive cells, 30–45 cone photoreceptor cell marker-positive cells, 30–100 horizontal and ganglion cell marker-positive cells, 40–140 bipolar cell marker-positive cells, and 30–60 Müller glial cell marker-positive cells for measuring infection efficiency for each retinal cell type. To show that AAV infection diffused throughout the retina, infection efficiencies in rod photoreceptor cells were calculated in the three areas, which are central, middle and peripheral areas to optic nerve head at the side uninjured by injection. Infection efficiencies in cone photoreceptor, bipolar, amacrine, and Müller glial cells were calculated in the central area. Infection efficiencies in horizontal and ganglion cells were calculated throughout the retina of the side uninjured by injection.

### Western Blot Analysis

Western blot analysis was performed as described previously [27]. The membrane was incubated with an anti-FLAG antibody (1:1000, F1804, Sigma). The membrane was then incubated with a horseradish peroxidase-conjugated goat antibody against mouse IgG (1:10000, Zymed). For the secondary immunoreaction, the PVDF membrane was incubated with WB Stripping Solution (Nacalai Tesque) to remove antibodies, and blocked again with 5% skim milk (wt/vol) in TBS. Further immunoblots were performed using a mouse antibody against  $\beta$ -actin (ACTB, 1:5000, Sigma).

### RT-qPCR

The mouse retinas were harvested and dissected at 3 weeks after injection. Total RNA (1  $\mu\text{g}$ ) from the retina was isolated using TRIzol reagent (Invitrogen) and converted to cDNA using Superscript II Reverse Transcriptase (Invitrogen). Real time PCR was performed using SYBR GreenER Q-PCR Super Mix (Invitrogen) and Thermal Cycler Dice Real Time System Single MRQ TP870 (Takara) according to the manufacturer's instructions. Quantification was performed by Thermal Cycler Dice Real Time System software version 2.0 (Takara). The primer sequences used for qPCR are listed in Table S1.

### ERG Recordings

Mice were anesthetized with an intramuscular injection of 80 mg/kg ketamine and 16 mg/kg xylazine. Pupils were dilated with topical 0.5% tropicamide and 0.5% phenylephrine HCl, and the mice were placed on a heating pad for the duration of the ERG recordings. ERGs were recorded with a gold wire loop placed on the cornea anesthetized with 1% tetracaine. A gold wire electrode was placed on the sclera 1 mm from the temporal limbus as the reference electrode. The mice were placed in a Ganzfeld bowl and 100 stroboscopic stimuli of 1.0 log cd-s/m<sup>2</sup> (PS33 Plus; Grass Telefactor) were averaged with a repetition rate of 1 sec to record the ERGs. Signals were amplified and bandpass filtered between 1 and 1000 Hz (Power Lab; AD Instruments, Castle Hill,

**Table 1.** Quantitative analysis of ERG amplitudes in control and AAV-Crx treated eyes.

	a-wave amplitudes	b-wave amplitudes
Control eye (6 weeks)		
1	0	0
2	0	0
3	0	0
AAV-treated eye (6 weeks)		
1	4.3	9.0
2	1.4	12.1
3	0	0
Control eye (15 weeks)		
1	0	0
2	0	0
3	0	0
AAV-treated eye (15 weeks)		
1	4.0	13.0
2	3.4	11.0
3	0	0

doi:10.1371/journal.pone.0054146.t001

Australia). Amplitudes of both a- and b-waves were quantified from photopic ERG responses.

### Transmission Electron Microscopy

Specimens for transmission electron microscopy were prepared in the following manner. Eyes were enucleated from anaesthetized mice. Following the removal of anterior segment, each posterior eyecup was fixed with 2% glutaraldehyde and 2% paraformaldehyde in a cacodylate-based buffer adjusted at pH 7.4. After fixation with 1% osmium tetroxide for 90 min, the retinas were dehydrated through a graded series of ethanol (50%–100%) and n-butylglycidylether. Finally, they were embedded in epoxy resin. Ultrathin sections were cut on an ultramicrotome (UltraCut E, Reichert-Jung, Vienna, Austria), and stained with uranyl acetate and lead citrate. Retinas were observed by transmission electron microscope (1200EX, JEOL, Japan).

### Statistical Analysis

Statistical significance was calculated with a Student's t test. A value of  $p < 0.05$  was taken to be statistically significant. Data are presented as means  $\pm$  SD.

### References

- Omori Y, Katoh K, Sato S, Muranishi Y, Chaya T, et al. (2011) Analysis of transcriptional regulatory pathways of photoreceptor genes by expression profiling of the *otx2*-deficient retina. *PLoS One* 6: e19685.
- Gamsiz ED, Ouyang Q, Schmidt M, Nagpal S, Morrow EM (2012) Genome-wide transcriptome analysis in murine neural retina using high-throughput RNA sequencing. *Genomics* 99: 44–51.
- Matsuda T, Cepko CL (2004) Electroporation and RNA interference in the rodent retina in vivo and in vitro. *Proc Natl Acad Sci U S A* 101: 16–22.
- Bostick B, Ghosh A, Yue Y, Long C, Duan D (2007) Systemic AAV-9 transduction in mice is influenced by animal age but not by the route of administration. *Gene Ther* 14: 1605–1609.
- Surace EM, Auricchio A, Reich SJ, Rex T, Glover E, et al. (2003) Delivery of adeno-associated virus vectors to the fetal retina: impact of viral capsid proteins on retinal neuronal progenitor transduction. *J Virol* 77: 7957–7963.
- Auricchio A, Kobinger G, Anand V, Hildinger M, O'Connor E, et al. (2001) Exchange of surface proteins impacts on viral vector cellular specificity and transduction characteristics: the retina as a model. *Hum Mol Genet* 10: 3075–3081.
- Allocca M, Mussolino C, Garcia-Hoyos M, Sanges D, Iodice C, et al. (2007) Novel adeno-associated virus serotypes efficiently transduce murine photoreceptors. *J Virol* 81: 11372–11380.
- Furukawa T, Morrow EM, Cepko CL (1997) *Crx*, a novel *otx*-like homeobox gene, shows photoreceptor-specific expression and regulates photoreceptor differentiation. *Cell* 91: 531–541.
- Chen S, Wang QL, Nie Z, Sun H, Lennon G, et al. (1997) *Crx*, a novel *Otx*-like paired-homeodomain protein, binds to and transactivates photoreceptor cell-specific genes. *Neuron* 19: 1017–1030.
- Furukawa T, Morrow EM, Li T, Davis FC, Cepko CL (1999) Retinopathy and attenuated circadian entrainment in *Crx*-deficient mice. *Nat Genet* 23: 466–470.
- Freund CL, Gregory-Evans CY, Furukawa T, Papaioannou M, Looser J, et al. (1997) Cone-rod dystrophy due to mutations in a novel photoreceptor-specific homeobox gene (*CRX*) essential for maintenance of the photoreceptor. *Cell* 91: 543–553.
- Swain PK, Chen S, Wang QL, Affatigato LM, Coats CL, et al. (1997) Mutations in the cone-rod homeobox gene are associated with the cone-rod dystrophy photoreceptor degeneration. *Neuron* 19: 1329–1336.
- Sohocki MM, Sullivan LS, Mintz-Hitner HA, Birch D, Heckenlively JR, et al. (1998) A range of clinical phenotypes associated with mutations in *CRX*, a photoreceptor transcription-factor gene. *Am J Hum Genet* 63: 1307–1315.
- Freund CL, Wang QL, Chen S, Muskat BL, Wiles CD, et al. (1998) De novo mutations in the *CRX* homeobox gene associated with Leber congenital amaurosis. *Nat Genet* 18: 311–312.
- Giove TJ, Sena-Esteves M, Eldred WD (2010) Transduction of the inner mouse retina using AAVrh8 and AAVrh10 via intravitreal injection. *Exp Eye Res* 91: 652–659.
- Mori S, Wang L, Takeuchi T, Kanda T (2004) Two novel adeno-associated viruses from cynomolgus monkey: pseudotyping characterization of capsid protein. *Virology* 330: 375–383.
- Furukawa A, Koike C, Lippincott P, Cepko CL, Furukawa T (2002) The mouse *Crx* 5'-upstream transgene sequence directs cell-specific and developmentally regulated expression in retinal photoreceptor cells. *J Neurosci* 22: 1640–1647.
- Koike C, Nishida A, Akimoto K, Nakaya MA, Noda T, et al. (2005) Function of atypical protein kinase C lambda in differentiating photoreceptors is required for proper lamination of mouse retina. *J Neurosci* 25: 10290–10298.
- Hsiao TH, Diaconu C, Myers CA, Lee J, Cepko CL, et al. (2007) The cis-regulatory logic of the mammalian photoreceptor transcriptional network. *PLoS One* 2: e643.
- Morrow EM, Furukawa T, Raviola E, Cepko CL (2005) Synaptogenesis and outer segment formation are perturbed in the neural retina of *Crx* mutant mice. *BMC Neurosci* 6: 5.
- Cepko CL, Austin CP, Yang X, Alexiades M, Ezzeddine D (1996) Cell fate determination in the vertebrate retina. *Proc Natl Acad Sci U S A* 93: 589–595.
- Gao G, Vandenberghe LH, Wilson JM (2005) New recombinant serotypes of AAV vectors. *Curr Gene Ther* 5: 285–297.
- Mears AJ, Kondo M, Swain PK, Takada Y, Bush RA, et al. (2001) *Nrl* is required for rod photoreceptor development. *Nat Genet* 29: 447–452.
- Chen J, Rattiner A, Nathans J (2005) The rod photoreceptor-specific nuclear receptor *Nr2e3* represses transcription of multiple cone-specific genes. *J Neurosci* 25: 118–129.
- Nishida A, Furukawa A, Koike C, Tano Y, Aizawa S, et al. (2003) *Otx2* homeobox gene controls retinal photoreceptor cell fate and pineal gland development. *Nat Neurosci* 6: 1255–1263.
- Niwa H, Yamamura K, Miyazaki J (1991) Efficient selection for high-expression transfectants with a novel eukaryotic vector. *Gene* 108: 193–199.
- Sanuki R, Onishi A, Koike C, Muramatsu R, Watanabe S, et al. (2011) miR-124a is required for hippocampal axogenesis and retinal cone survival through *Lhx2* suppression. *Nat Neurosci* 14: 1125–1134.
- Muranishi Y, Terada K, Inoue T, Katoh K, Tsujii T, et al. (2011) An Essential Role for RAX Homeoprotein and NOTCH-HES Signaling in *Otx2* Expression in Embryonic Retinal Photoreceptor Cell Fate Determination. *J Neurosci* 31: 16792–16807.
- de Melo J, Blackshaw S (2011) In vivo electroporation of developing mouse retina. *J Vis Exp* 52: pii 2847.

### Supporting Information

**Table S1 Primer sequences.** Primers for qPCR analysis. (XLS)

### Acknowledgments

We thank J. Johnston for the *pAAV2/1*, *pXR5*, *pAAV2/8*, *pAAV2/9*, and *pAAV2/rh10* vectors, and S. Mori for the *pEEV2/11* vector. We thank Y. Chérrase for help in producing the AAV. We thank Y. Omori, A. Onishi, Y. Muranishi, T. Chaya and S. Irie for critical comments and technical advice, and A. Tani, M. Kadowaki, A. Ishimaru, H. Tsujii, Y. Saioka, H. Abe, and S. Kennedy for technical assistance.

### Author Contributions

Conceived and designed the experiments: TF SW RS. Performed the experiments: SW RS SU TK TH. Analyzed the data: SW TF RS SU TH. Contributed reagents/materials/analysis tools: TF SU TH. Wrote the paper: SW TF.